Journal of Crystal Growth 634 (2024) 127606

Contents lists available at ScienceDirect

Journal of Crystal Growth

journal homepage: www.elsevier.com/locate/jcrysgro

Invited Review

Solid solution perovskite substrate materials with indifferent points

Vincent J. Fratello [a,*], Lynn A. Boatner [b], Hanna A. Dabkowska [c], Antoni Dabkowski [c], Theo Siegrist [d], Kaya Wei [d], Christo Guguschev [e], Detlef Klimm [e], Mario Brützam [e], Darrell G. Schlom [f,g,e], Shanthi Subramanian [h]

[a] Quest Integrity USA, A Baker-Hughes Company, Renton, Washington, USA
[b] Oak Ridge National Laboratory, USA
[c] McMaster University, Canada
[d] National High Magnetic Field Laboratory and Florida State University, USA
[e] Leibniz-Institut für Kristallzüchtung, Max-Born-Str. 2, 12489 Berlin, Germany
[f] Department of Materials Science and Engineering, Cornell University, Ithaca, NY 14853, USA
[g] Kavli Institute at Cornell for Nanoscale Science, Ithaca, New York 14853, USA
[h] Coherent, Incorporated

ARTICLE INFO

Communicated by Jeffrey Derby

Keywords:
A1. Phase diagrams
A1. Solid solutions
A1. Substrates
A2. Growth from melt
A2. Single crystal growth
B1. Perovskites

ABSTRACT

Single-crystal substrate materials with crystal structures and lattice parameters matching a desired epitaxial film are an enabling technology for many critical materials. Such substrates are best grown by bulk techniques that benefit from the substrate material being congruently melting. The shortage of congruently melting perovskites in critical lattice parameter ranges has been addressed herein by a search for new congruently melting compositions. A solid solution of two perovskites can be congruently melting at a minimum temperature under specified thermodynamic conditions where the coefficient matrix has a zero determinant. This is called an indifferent point. A wide variety of perovskite solid solutions were investigated to identify compounds that have an indifferent melting minimum and a cubic crystal structure with favorable lattice constants in the range of 0.390–0.412 nm. Solid solution pairs that form such indifferent points include, but are not limited to, seven compositions identified in this study. The lattice parameters of the new materials show a broad range of desirable lattice constants. A perovskite tolerance factor close to unity gave a favorable contribution to the free energy and makes a cubic crystal structure favorable. These solid solutions constitute a broad and important class of compounds not previously anticipated. The only significant drawback is the high vapor pressure of sodium, which is present in most of these materials and requires special growth conditions and equipment for safety.

1. Introduction

Archimedes is quoted as saying "Give me a place to stand and I will move the earth." Such is the role of a substrate in epitaxial crystal growth. In a small number of cases, thermodynamics is favorable, and a large uniform crystal of a congruently melting composition can be grown by some bulk method at a reasonable temperature. But if the desired material is non-congruent, has a high melting temperature, contains volatile ingredients, or the crystal is desired in a thin film or multilayer form that is not self-supporting, then epitaxy is the required method of growth. Thin films may be grown by vapor phase means such as molecular-beam epitaxy or metal–organic chemical vapor deposition, while thick films require more rapid liquid phase epitaxy from a high-temperature solution. All these methods require a high-quality substrate that is a good structure and lattice parameter match to the film.

Perovskites are the most abundant mineral inside our planet and constitute most of Earth's lower mantle. They are isostructural with the mineral perovskite ($CaTiO_3$), but the perovskite crystal structure is really a generic structure defined by a network of anions with cube-octahedral (12-sided) and corner-sharing octahedral (8-sided) cation sites. The most common nominal perovskite formula is ABO_3, though other anions are possible and off-stoichiometry compounds with vacancies occur. The cation sites in the anion structure can accommodate over half the metal cations in the periodic table and still retain the perovskite structure, but with properties that Mother Nature never produced. The average cation valence of the A and B sites in

* Corresponding author.
E-mail address: vjfratello@gmail.com (V.J. Fratello).

https://doi.org/10.1016/j.jcrysgro.2024.127606
Received 9 October 2023; Received in revised form 29 January 2024; Accepted 30 January 2024
Available online 3 February 2024

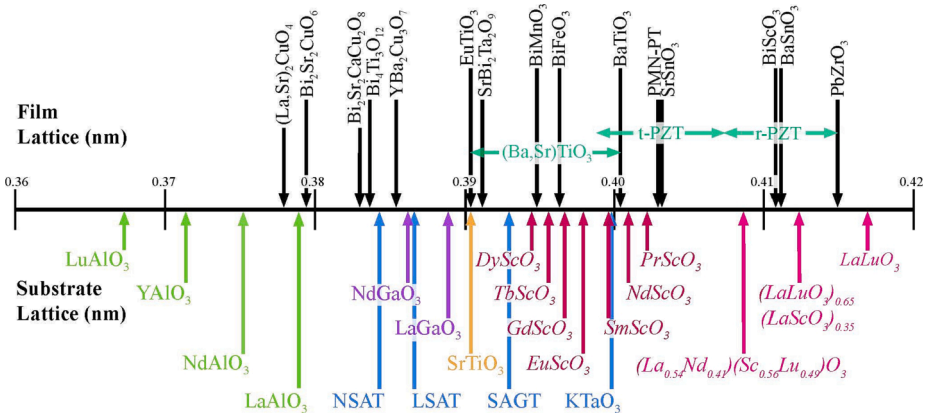

Fig. 1. Primitive perovskite lattice parameters of some desired epitaxial single crystal films (above the number line) and currently available prior art substrate materials (below the number line).[1] The aluminates are in green, the tantalates are in blue, the gallates are in purple, the titanates are in yellow, the scandates are in dark red and italicized and solid solutions containing $LaLuO_3$ are in magenta and italicized. The italicized entries have expensive constituents, require iridium crucibles, and are impractical for commercial use. (For interpretation of the references to colour in this figure legend, the reader is referred to the web version of this article.)

stoichiometric ABO_3 must be 3+, but this can be achieved by $A^{1+}B^{5+}$, $A^{2+}B^{4+}$, $A^{3+}B^{3+}$ or more complex chemistries with multiple A site ions, multiple B site ions, vacancies, etc. Perovskites comprise technologically important materials because they can be ferroelectric, electrooptic, ferromagnetic, ferrimagnetic, antiferromagnetic, multiferroic, piezoelectric, pyroelectric, paraelectric, magnetoresistive, colossal magnetoresistive, magnetooptic, photovoltaic, photoluminescent, insulating, conducting, semiconducting, superconducting, ferroelastic, magnetostrictive, catalytic, etc. Researchers have developed complex perovskite multilayer thin films for potential devices ranging from spintronics to ferroelectric transistors. Unfortunately, there are limits to the available commercial substrates for film growth with most substrates being small, expensive, and limited in availability.

Fig. 1 depicts a prior art plot of known substrate materials (bottom) and some film materials (top) plotted on the average lattice parameter number line for the simple perovskite single formula unit ABO_3 unit cell. Note that some of these materials, especially in the epitaxial category, have actual unit cells that are more complex with multiple lattice parameters including integer multiples of the simple unit cell and $\sqrt{2}$ or even higher order square root multiples of the lattice parameter(s) when the unit cell is rotated, but for the purposes of comparison in this plot, the lattice parameters are all converted to the simple primitive/reduced perovskite unit cell of one ABO_3 formula unit with an average lattice parameter of the cube root of the volume per formula unit.

As can be seen from this plot, there are substrate candidates with primitive lattice parameters from 0.367 to 0.417 nm, however, above 0.387 nm there is a dearth of cubic materials that may be readily grown in large size. Problems with existing compounds on the number line in this range are discussed below.

- The rare-earth scandates $DyScO_3$ through $PrScO_3$, the similar compounds (La,Nd)(Sc,Lu)O_3 and $LaLuO_3$ and more recent high melting temperature materials can be grown as single crystals by the Czochralski method. Scandium oxide and the rare-earth oxides are highly refractory materials, and the rare-earth scandates have extremely high melting temperatures close to the 2200 °C limit of Czochralski growth from an iridium crucible. Scandium is also a rare-earth group metal with limited availability and a high price, and the other rare-earth constituents are expensive in varying degrees and can have limited availability. These rare-earth scandate substrate materials are only available in limited quantities for research studies, are small, typically 1 cm square to 3.4 cm diameter round, and are expensive.
- Potassium tantalate $KTaO_3$ is peritectic rather than congruently melting and has been grown from an off-stoichiometry melt for scientific samples. The sizes available range from 5 to 20 mm, which are too small for a commercial product, and the available substrates are expensive with limited sources, mostly non-commercial.
- Strontium aluminum gallium tantalate SAGT is a conventional solid solution and any crystal grown will have a compositional and lattice parameter gradient especially as the crystal size and fraction of the melt that has grown increase.
- Strontium titanate $SrTiO_3$ has a high melting point and is readily reduced unless the growth atmosphere is highly oxidizing, or the growth temperature is lowered by use of a flux or solvent. Crystals are commercially prepared by flame-fusion growth and have also been grown experimentally from KF—LiF and K-Li-borate fluxes. Neither of these techniques is amenable to the growth of large crystals, and this material is also expensive.
- Lanthanum gallate $LaGaO_3$ and neodymium gallate $NdGaO_3$ are not cubic and are subject to twinning.

So, for any commercial technology there is a virtual valley in the lattice parameter number line with no viable, large-size, commercial, congruently-melting, cubic perovskite substrate candidates. This is a substantial pain point to developing new technologies. There have been long-term efforts to characterize the known composition space of simple and complex perovskites and those options are reaching their limits. Therefore, new materials outside the scope of straightforward combinatorics are required to permit growth of epitaxial crystals with a good lattice match in this lattice parameter range.

2. Solid solutions

A solid solution is a mixture of two substances that can exist as a solid over a range of proportions between the two end members such that the crystal structure remains unchanged or is only slightly distorted by the addition of the other end member. Even though all these materials are solids, this can be thought of as one substance (the solute) being added to another (the solvent). If the two end members have the same crystal structure, their constituents can fill the atomic sites of this structure by substitution, and all possible proportions between the two end members are homogeneous crystals of that structure, then this is described as a continuous solid solution. In this way, neither end member is exclusively the solvent or the solute. Solid solutions are typically thought of as disordered, whereas a perfectly ordered stoichiometric mixture is a compound with a fixed composition or range of compositions.

Nevertheless, varying degrees of order, disorder, homogeneity, and inhomogeneity including clustering may be present over the range of compositions in a solid solution.

Because of the common structure, solid solutions readily form between two perovskites, where two end members, e.g., ABO_3 and $A'B'O_3$ may mix with fractions $0 < x < 1$ to a range of ordered, partially ordered, and disordered materials $A_xA'_{1-x}B_xB'_{1-x}O_3$. If $A = A'$, this is simplified to $AB_xB'_{1-x}O_3$ as is the case for some of the materials discussed in this work. If A and A′ or B and B′ are different in valence, constraints of stoichiometry allow this to be viewed in a first approximation as a two-component pseudo-binary solid solution, though real compounds can have vacancies, anti-site ions, impurities, dopants, and other defects. There are cases where one or more ions may be present on both the A and B sites, which allows an additional degree of freedom. Because solid solutions are not line compounds with a fixed composition, these commonly have complex melting and crystallization behaviors as discussed below.

For this simple illustration, there is assumed to be no dependence of the enthalpies of crystallization/melting on temperature T and the solid and liquid entropies of mixing ΔS_m are assumed equal. The excess free energy of the liquid is given by its entropy of mixing:

$$\Delta G_L = -T\Delta S_m. \tag{1}$$

The free energy of the solid ΔG_S is given by the linear combination of the temperature-dependent free energies of the end members $(1-x)\Delta G_C + x\Delta G_D$ plus the free energy of mixing $\Delta G_m = \Delta H_m - T\Delta S_m$:

$$\Delta G_S = (1-x)\Delta G_C + x\Delta G_D + \Delta H_m - T\Delta S_m. \tag{2}$$

This solid free energy curve shifts up and down as the temperature varies. The simplified form of the entropy of mixing ΔS_m term for a proportion x is assumed to be as shown in Eqn. (3),

$$-T\Delta S_m = RT(x\ln(x) + (1-x)\ln(1-x)) \tag{3}$$

where R is the universal gas constant and ln is the natural logarithm.

2.1. Simple solid solution

Fig. 2 depicts construction of a simple binary solid solution phase diagram. The free energy diagram is given by the free energy of crystallization of the two end members C and D and the entropy of mixing terms ΔS_m in the liquid and solid. For a simple solid solution it is assumed that there is no enthalpy of mixing in the solid so that C and D can be randomly distributed with no preference for order or disorder but tending toward good mixing because of entropy.

The solid and liquid free energy curves can only be tangent at the same composition at the end members. Therefore, the compound that crystallizes at any composition will be biased toward the higher melting compound. The farther apart the two melting points are, the more the liquidus (temperature where the last solid phase melts on heating or the first solid phase appears on cooling) deviates from the solidus (temperature where the last liquid phase solidifies on cooling or the first liquid phase appears on heating), and therefore more segregation occurs. A crystal grown in this way by cooling along the liquidus curve will have a continuously varying composition, properties, and, if the ions are of different sizes, variable lattice parameter through the length and be of limited technological use. Two phases (solid and liquid) are in equilibrium on the solidus and liquidus lines.

2.2. Eutectic

The enthalpy of mixing ΔH_m in a simple C—D mixture can be approximated in terms of the enthalpy of adjacent bonds between two C atoms, H_{CC}, two D atoms, H_{DD} and C and D atoms, H_{CD}:

$$\Delta H_m = x(1-x)[H_{CD} - (H_{CC} + H_{DD})/2] \tag{4}$$

If the enthalpy of the C-D bond is higher than the average of the C–C and D-D bonds, which is to say it is unfavorable for C and D to be adjacent, then the enthalpy of mixing is positive (thermodynamically unfavorable), and it counteracts the free-energy contribution of the entropy of mixing. These terms contain the thermodynamic contributions of stress and electromagnetic interactions among the various ions but to calculate those explicitly for multiple ions of differing signs and valences on each site is beyond the scope of this paper. If there is a significant positive enthalpy of mixing in the crystal, complete unmixing and phase separation occurs in the middle of the phase diagram where the enthalpy of mixing is highest. This is called a eutectic and is depicted in Fig. 3. The different functional forms of the free energy terms of the entropy and enthalpy of mixing result in a complex free energy curve of the solid solution with two local minima that has its lowest free energy for a mixture of the two terminal solid solutions SSγ (a solid solution of D in C) and SSδ (a solid solution of C in D). At the eutectic point, this phase separation results in three phases in equilibrium, the liquid, SSγ, and SSδ consistent with Gibbs' phase rule.

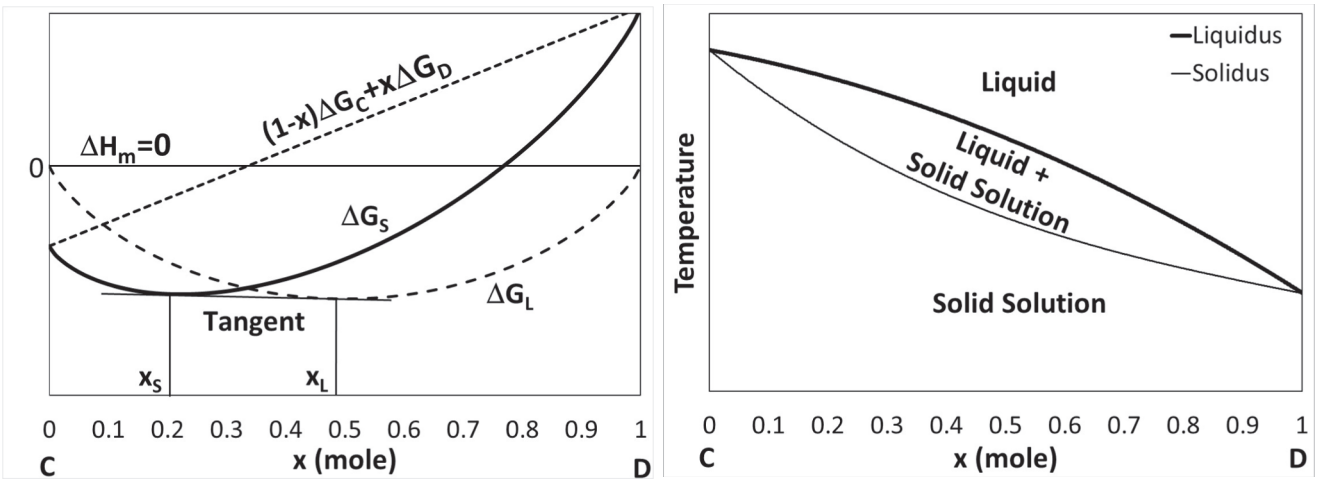

Fig. 2. Construction of a phase diagram of a simple solid solution with no enthalpy of mixing $\Delta H_m = 0$. A large $\Delta G_D - \Delta G_C = 1.25RT$ was used to make the split more obvious. (a) Free energy diagram with mutual tangent. (b) Phase diagram of a continuous solid solution.

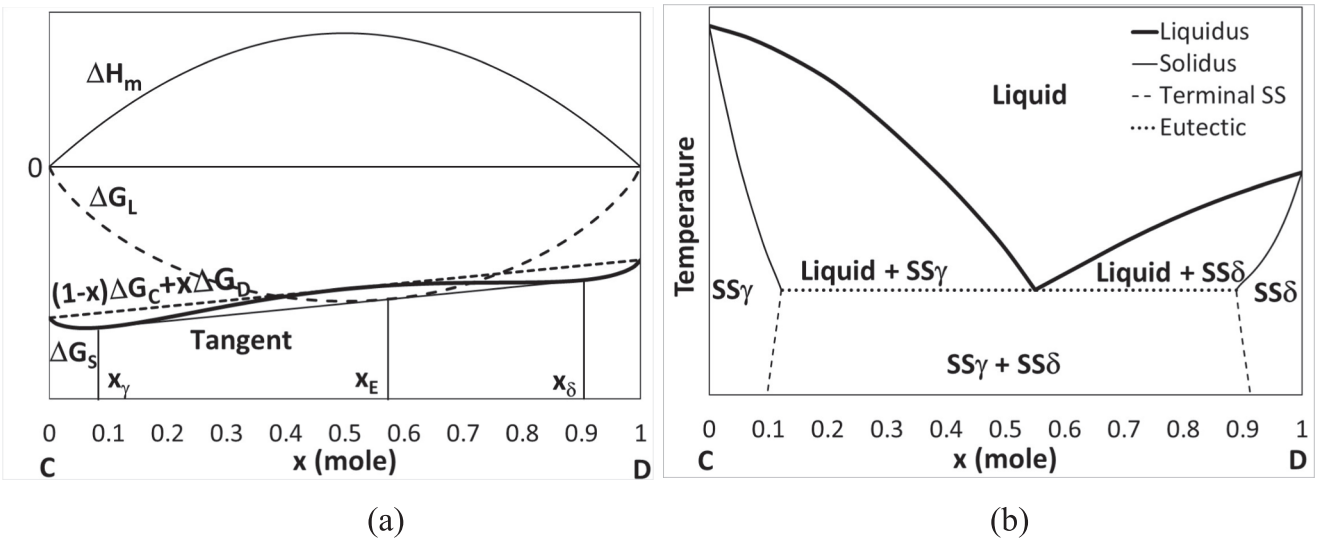

Fig. 3. Construction of a eutectic phase diagram resulting from a positive enthalpy of mixing. (a) Free energy diagram with mutual tangent at two points on the solid free energy curve. The enthalpy of mixing coefficient is $[H_{CD}-(H_{CC}+H_{DD})/2] = 2.77RT$ and $\Delta G_D - \Delta G_C = 0.3RT$. (b) Phase diagram of a eutectic.

2.3. Gibbs' phase rule

Gibbs' phase rule defines the number of phases Π in a materials system at equilibrium as a relation between the rank of the coefficient matrix N (equal to the number of independent components in the system) and the degrees of freedom F of the equilibrium condition. Typically, N is taken to be equal to the number of components. In this case, pressure is constant, and the only variables are composition and temperature, thus the so-called "condensed" phase rule applies:

$$\Pi = N - F + 1 \tag{5}$$

In a constrained pseudo-binary phase diagram, it is the common teaching of the phase rule that $N = 2$ and under these circumstances, two phases ($\Pi = 2$) can come together on an equilibrium line ($F = 1$), but an equilibrium point ($F = 0$) requires the meeting of three phases ($\Pi = 3$). (It is pseudo-binary because there are more potential degrees of freedom taken to be fixed by constraints of stoichiometry, ambient pressure, etc.)

A small number of continuous solid solutions have a unique feature where the liquidus and solidus curves come together at a congruently melting maximum or minimum at some fixed proportion. This is referred to as an azeotrope in vapor–liquid systems, which include the well-known ethanol–water system. For liquid–solid systems, it is properly referred to as an indifferent point and this point constitutes congruent melting. There are a substantial number of alkali halides that display this behavior, but few perovskites that have a congruently melting minimum have been recorded to date. Some discussion is required to understand how these situations comply with Gibbs' phase rule.

2.4. Congruently melting maximum

If, instead of the eutectic example above, the enthalpy of the C-D bond is lower than the average of the C-C and D-D bonds, then the enthalpy of mixing is negative (more thermodynamically favorable), and it is favorable for C and D atoms to be adjacent, reinforcing the free energy contribution of the entropy of mixing. In an imaginary C-D compound this could result in perfect C-D-C-D ordering with a higher order unit cell. Complex $AB_xB'_{1-x}O_3$ perovskites can have different stoichiometries such as 1:1, 2:1 (depicted in Fig. 4), 3:1 and even non-integer mixtures.

Once again, the difference in functional forms of the entropy and

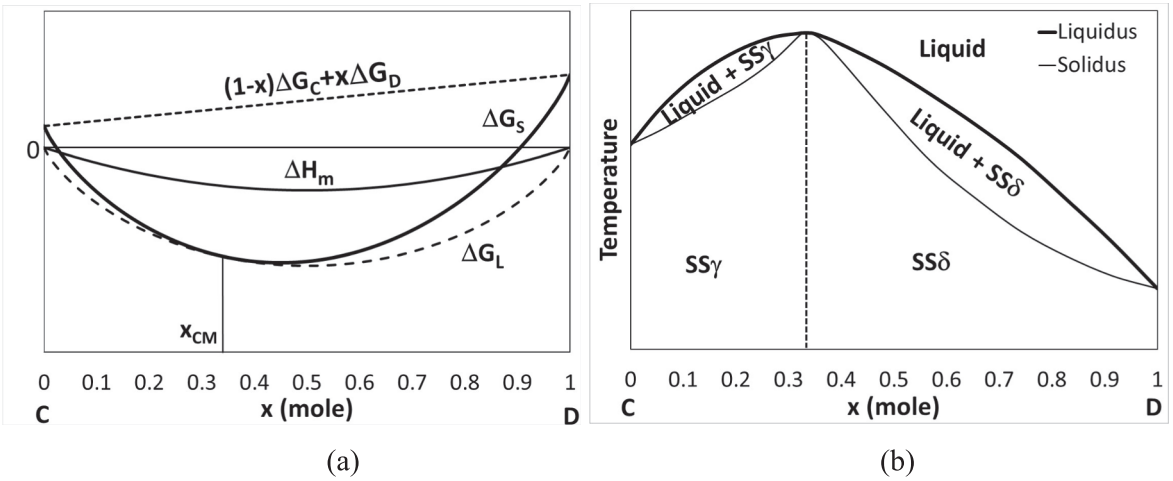

Fig. 4. Construction of a phase diagram with a congruently melting 2:1 (33 %) maximum resulting from a negative enthalpy of mixing. (a) Free energy diagram with mutual tangent at a point. The enthalpy of mixing coefficient is $[H_{CD} - (H_{CC} + H_{DD})/2] = -RT$ and $\Delta G_D - \Delta G_C = 0.3RT$. (b) Phase diagram of a congruently melting compound.

enthalpy of mixing allow a different free-energy curve, in this case the solid curve is above the liquid curve at all points with a tangent point in the middle. In this formulation, a negative enthalpy of mixing is a prerequisite for the congruent maximum at x_{CM}. The necessary criterion for an indifferent point is $d(\Delta G_S - \Delta G_L)/dx = 0$ in Fig. 4a, which is satisfied by ΔG_S and ΔG_L having the same slope at the congruent point per the construction in Fig. 4a, and results in the congruent condition $dT/dx = 0$ at x_{CM} in Fig. 4b. Inserting the relevant quantities and solving for the maximum point x_{CM} gives:

$$x_{CM} = 0.5(\Delta G_D - \Delta G_C)/[H_{CD} - (H_{CC} + H_{DD})/2] + 0.5 \quad (6)$$

The maximum point comes closer to $x = 0.5$ for a larger negative mixing coefficient $[H_{CD} - (H_{CC} + H_{DD})/2]$ and closer to the higher melting end member for smaller negative $[H_{CD} - (H_{CC} + H_{DD})/2]$ reaching the axis for zero enthalpy of mixing $[H_{CD} - (H_{CC} + H_{DD})/2] = 0$, resulting in a simple solid solution phase diagram as in Fig. 2.

It has been argued previously that this ordering transition disambiguates between solid solutions SSγ (a solid solution of D in C) and SSδ (a solid solution of C in D), such that at the congruent point they come together as two solid solutions with the same composition[2], thereby satisfying the conventional form of the condensed phase rule. The argument that SSγ and SSδ remain distinct gives three phases with the liquid at the congruent melting point. A crystallizing composition away from the congruent maximum will move away from the congruent composition as crystallization progresses.

2.5. Congruently melting minimum

There is another case to be considered. If the enthalpy of mixing is positive, but small, it may not be sufficient to overcome the entropy of mixing at the melting temperature, and there is only a single flattened minimum. Once again, the difference in functional forms of the entropy and enthalpy of mixing allow a different free-energy curve, in this case the solid curve is below the liquid curve at all points with a tangent point in the middle as in Fig. 5a. This results in a congruent melting minimum as in Fig. 5b. For this condition, a crystallizing composition away from the congruent minimum will move toward the congruent composition as crystallization progresses.

There can still be phase separation of the solid solution below the solidus because the negative entropy of mixing term will reduce in magnitude with temperature to be of lower magnitude than the positive enthalpy of mixing, giving a temperature where the free energy of mixing changes from negative above to positive below, and this can result in solid phase spinodal decomposition/phase separation that is destructive if it occurs at a temperature where the ions are sufficiently mobile for the transformation to occur. Therefore, returning a congruently grown crystal intact to room temperature either requires that the decomposition temperature be below room temperature or at such a low temperature that the atoms are "frozen" in place and phase separation in any realistic time is kinetically impossible. This further constrains which systems can successfully produce crystals.

Interestingly, at the congruent temperature there appears to be only a single continuous solid solution phase and only two phases at the congruent point, seeming to violate the phase rule. While it is possible that there are clustering terms that provide some higher degree of order that could once again disambiguate the two solid solutions, it is not necessary if the full definition of the phase rule is considered.

2.6. Indifferent points

The requirements for an indifferent point to occur must be discussed in terms of the full definition of Gibbs' phase rule. This is often oversimplified in the literature, and therefore its application is explained briefly here. As discussed above, N is typically taken to be equal to the number of components, but that oversimplification loses information critical to understanding indifferent points.

The problem arises in the assumption that $N = 2$ for two components. The number of independent components is actually the rank of the coefficient matrix. The rank of the coefficient matrix equals the number of components if the determinant is non-zero. If the state in question strictly minimizes the total internal energy in the sense of Gibbs' minimum energy principle, then the rank of the coefficient matrix equals the number of components and Gibbs' traditional phase rule is valid ($N = 2$ here).[3] Nonetheless, the coefficient matrix for some binary mixtures can mathematically have a zero determinant at some composition, in which case the coefficient matrix rank is 1 (same as the equations not being independent). In this case, the matrix form of the Gibbs-Duhem equation does not require that all differential chemical potentials be zero ($d\mu = 0$) and that the total internal energy be minimized. Federov classified such acnodes in phase diagrams.[4] Tester and Modell suggest that the phase rule must be interpreted to mean that "there are certain sets of intensive properties which, when selected, will completely define

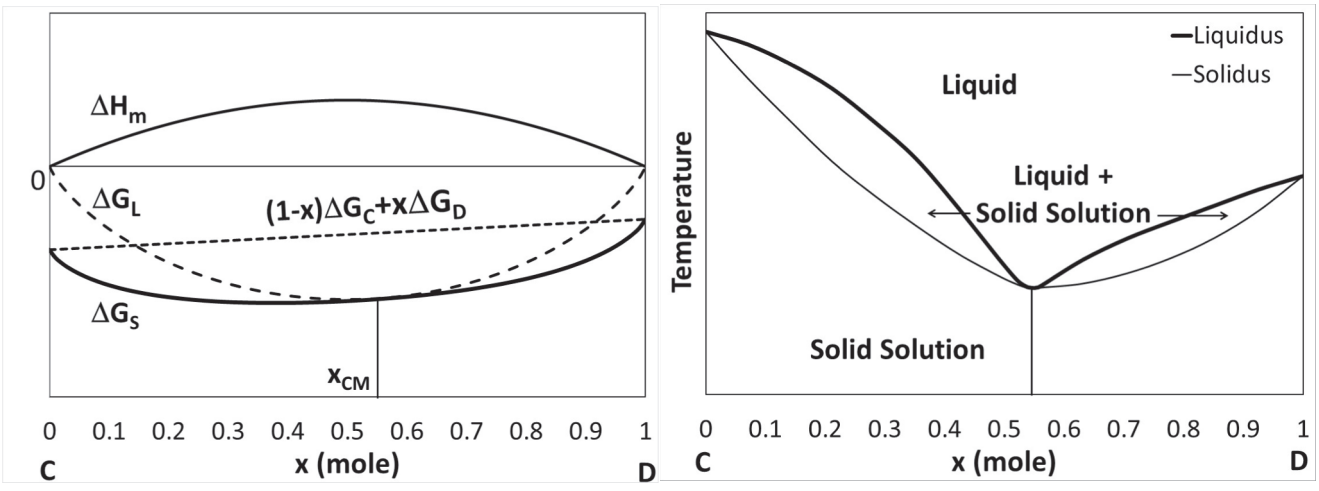

Fig. 5. Construction of a phase diagram with a congruently melting minimum resulting from a small positive enthalpy of mixing. (a) Free energy diagram with mutual tangent at a point. The enthalpy of mixing coefficient is $[H_{CD} - (H_{CC} + H_{DD})/2] = 1.385RT$. A smaller $\Delta G_D - \Delta G_C = 0.16RT$ was needed to keep this near the center of the phase diagram. (b) Phase diagram of a congruently melting minimum at an indifferent point.

the system" but there is not freedom to choose any set.[5] Mathematically, this critical point of the defining polynomial function is referred to as an acnode or singularity where the function must have a local minimum or maximum. This is the condition that permits an indifferent point in a solution/solid solution.

Unfortunately, the mathematical condition of a zero determinant does not usefully predict which chemical systems will have such an indifferent point. Therefore, the purpose of this study is to determine what conditions empirically yield an indifferent point, specifically with a congruently melting minimum.

2.7. Known perovskite solid solutions with an indifferent point

$BaTiO_3$—$CaTiO_3$ – Such a congruent minimum is depicted in Fig. 6 for a continuous solid solution between the perovskites barium titanate $BaTiO_3$ and calcium titanate $CaTiO_3$.[6] The congruent nature of this material was verified by other authors from the growth of single crystals and determination of the uniformity of composition along the crystal length. No distinction is made by the authors between the high-temperature cubic phases on the right and left sides of the congruent point. The congruent composition transforms to a tetragonal phase at 98 °C, so this material is not appropriate as a substrate. This $A_xA'_{1-x}BO_3$ solid solution has A = Ba and A′ = Ca with the same valence 2+ and B = Ti in the 4+ valence state. Having two A ions of the same valence

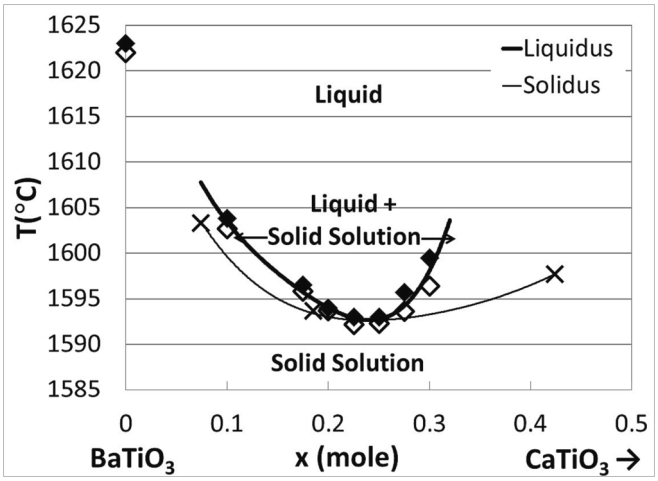

Fig. 6. Pseudo-binary phase diagram of $BaTiO_3$—$CaTiO_3$.[6] On the liquidus, solid diamonds denote where complete melting occurs on heating and open diamonds denote where crystallization begins on cooling. The crosses are x-ray fluorescence data on resultant crystals on the solidus.

simplifies the solid solution in this case because the different sizes of the two ions can create a positive enthalpy of mixing, but in others, where the two A-site ions of the same valence are more similar in size, there is redundancy and an additional degree of freedom.

$REAlO_3$—$AEAl_{1/2}Ta_{1/2}O_3$ and $REAlO_3$—$AEAl_{1/2}Nb_{1/2}O_3$ – Mateika and co-workers found congruent or near-congruent compositions by putting paired "guest ions" in $REAlO_3$ perovskites. These are actually solid solutions between $REAlO_3$ and $AEAl_{1/2}B'_{1/2}O_3$ where the alkaline earth AE was Sr or Ca and B′ was Ta or Nb.[7] This is a more complex solid solution because Al is in both end members but is not the only B ion. The proportions are constrained to a single variable x by the ionic valences and the fact that all species are single-site ions, so this remains a pseudo-binary. The compositions are $xREAlO_3$—$(1-x)AEAl_{1/2}B'_{1/2}O_3$ or $RE_xAE_{1-x}Al_{(1+x)/2}B'_{(1-x)/2}O_3$. The compounds with Sr and La/Pr/Nd were cubic, while the others took on a variety of structures. The multiple solid solutions with Ca and Sr substituted together or two rare earths substituted together were near-congruent, but not perfectly so, possibly because of the additional degree of freedom. A substrate material of technological importance from this system that has a continuous solid solution with a congruent minimum is the cubic perovskite solid solution between a simple perovskite lanthanum aluminate $LaAlO_3$ and the complex perovskite strontium aluminum tantalate $SrAl_{1/2}Ta_{1/2}O_3$ (listed as LSAT in the bottom of Fig. 1 as a substrate). This compound has a previously measured congruently melting minimum temperature of ~ 1820 °C at $x \approx 0.23$.[8] The range of congruency given on the phase diagram may result from the tendency of compositions off a congruent minimum to move towards the congruent composition during growth. The congruent nature of this material was verified by the growth of single crystals, determination of the uniformity of composition along the crystal length, and comparison to the residual melt. The crystal structure remains unchanged to 700 °C. This material has a reported lattice parameter of ~ 0.3865 nm at the congruent composition and is used as a substrate for high-temperature superconductors and other applications. Other cubic crystals of this family $(PrAlO_3)_{0.38}$—$(SrAl_{1/2}Ta_{1/2}O_3)_{0.62}$ (PSAT) and $(NdAlO_3)_{0.39}$—$(SrAl_{1/2}Ta_{1/2}O_3)_{0.61}$ (NSAT) have lower lattice parameters. None of the reported compositions had an optimized Goldschmidt perovskite tolerance factor [9] equal to 1.

$BaTiO_3$—$NaNbO_3$ – The continuous solid solution perovskite between barium titanate $BaTiO_3$ (BT) and sodium niobate $NaNbO_3$ (NN), BT—NN, was identified as having a similar congruently melting minimum. The available prior art melting curve phase diagrams in Fig. 7a and Fig. 7b differ in the position of the congruent point between 50 and 60 mol percent $BaTiO_3$ (x = 0.5–0.6), which, respectively, have tolerance factors t of 1.014 and 1.023 utilizing the "crystal radii" of Shannon [10].

This material has not been grown in single-crystal form, and nothing further about it is given in the literature beyond its initial discovery. No

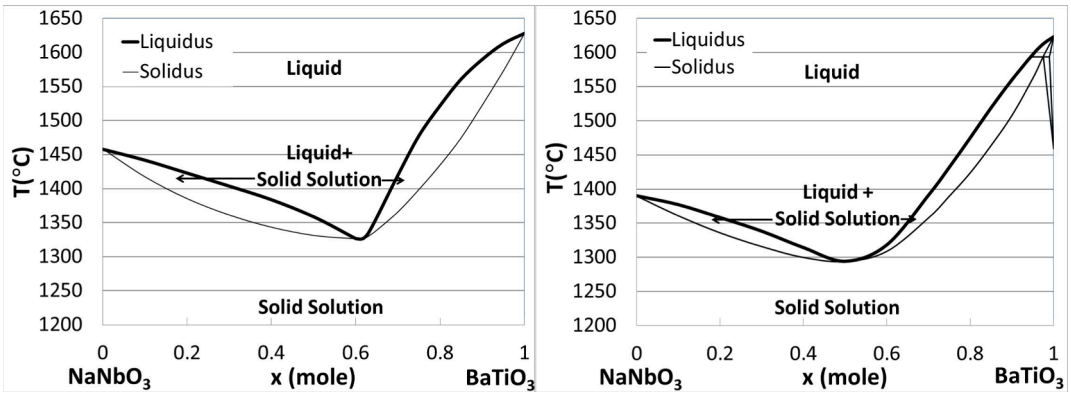

Fig. 7. Prior art preliminary pseudo-binary phase diagrams of $NaNbO_3$—$BaTiO_3$. (a) D. E. Rase and R. Roy [11], (b) Merrill W. Schaefer [12].

determination of the high-temperature phase structure was made. This material is a solid solution on both A and B sites $A_xA'_{1-x}B_xB'_{1-x}O_3$ where the pairs A = Ba, A′ = Na and B = Ti, B′ = Nb have differing valences and therefore must be matched in proportion x if the conditions are met that the compound is stoichiometric, all ions are single site, and there are no significant vacancies or other stoichiometry defects. Therefore this too is pseudo-binary.

3. Experimental

While there are many materials with the perovskite crystal structure in the literature, this study was limited to compounds that have the following traits that were determined to give the best odds of a cubic congruently melting substrate material in the desired lattice parameter range.

- *Near unity tolerance factor*. The phase stability and crystallographic structure of perovskites depend on the relation between the average ionic sizes on the two sites in the crystal. The ease of formation of an oxide perovskite for any A—B pair depends on the crystal ionic radii or, in the case of more complex structures, averaged site crystal ionic radii, and is given by the dimensionless Goldschmidt perovskite tolerance factor[9]:

$$t = (r_A + r_O)/(r_B + r_O)/\sqrt{2} \tag{7}$$

  where r_A and r_B are the average A- and B-site ionic radii and r_O is the oxygen ionic radius. Goldschmidt[9] observed that stability of the perovskite structure may be found within the limits $t = 0.77$ to 0.99, and others have extended that to 0.71 to 1.09, but cubic symmetry is best found near unity $t = 1.00$. The "crystal radii" of Shannon[10] are used herein for r_A and r_B since they best represent the situation in the perovskite rather than the free ionic radii, and r_O is 0.126 nm[10]. In the current study, the best congruency was seen to occur for t = 0.98–1.02. Some of the end member compounds have high or low tolerance factors and are not cubic, but blending compounds of higher and lower tolerance factors achieves a solid solution with t close to unity in the mixture, which favors a cubic structure of the solid solution at the congruent composition. The tolerance factor t can contribute to a thermodynamic energy minimum, and it was found that this can shift the melting point depression curves of the end members' solid solutions and therefore the position of the minimum. The tolerance factor of the actual indifferent point was at worst the same and mostly closer to unity than the predicted value.
- *Stable end member compounds*. If the end members are stable and preferentially congruently melting, the solid solution is more likely to be so as well.
- *Common ions*. Having a common ion or ions among the two end member compounds reduces the number of degrees of freedom.
- *Compatible crystal ionic sizes*. It has been noted that compounds are less stable if the relative ion sizes cause a lattice expansion owing to the relatively larger ion on the cube-octahedral site that allows the relatively smaller ion to "rattle around" in the octahedral site. For example, aluminum on the B-site is not compatible with barium on the A-site as Al is simply too small for the octahedral site in a Ba-based perovskite. On the other hand, lithium is large for the octahedral site in a perovskite with only Sr on the A site and tends to distort the lattice.
- *Low to moderate vapor pressure of all constituents to stabilize the melt*. In practice, the vapor pressures of species such as sodium and nickel can be compensated by adding an extra amount of these components, adjusting the oxygen concentration of the atmosphere, or using a closed vessel, while those of potassium, tin, and indium are too high for most growth conditions. The use of sodium is addressed below.
- *Not excessively refractory*. The zirconates, for example, are well known perovskites but have such high melting points that they cannot be grown in bulk by practical means. Scandium and magnesium were avoided similarly as, for example, $BaMg_{1/3}Nb_{2/3}O_3$ melts at 2900 °C. Reasons to keep these melting points low are multi-fold.
  - An indifferent point cannot be achieved if the two components have too high a difference in melting temperatures.
  - Constituents such as Ti, Nb, and Ta can be reduced at high temperatures, so a melting temperature is desired < 1800 °C and preferentially < 1600 °C, where a platinum crucible and air or another oxidizing atmosphere can be used.
  - Higher temperatures obviously increase the vapor pressure of moderately volatile constituents.
- *Limited concentrations of ions empirically observed to result in distortion or phase separation*. These were found in this study to include, but were not limited to, Al in Ba-containing compounds (phase separation), Ga (phase separation), and Li (non-cubic distortion).
- *Avoiding ions of the same valence on a single site*. This can result in another degree of freedom, but in simple compounds had mixed results. While BT—CT is a successful congruently melting solid solution with a single degree of freedom and an indifferent point, BT—ST is not. Ions of the same valence on a single site gave redundancy in possible compositions particularly if the composition involved same-valence cations on both the A and B sites. Solid solutions between barium A and strontium A′ with the Sr compound having $t < 1$ and the Ba compound having $t > 1$ tended to form ordinary solid solutions because there was no negative heat of mixing. The ions are too similar in size/valence. A number of potential Ba—Sr solid solutions in this study (as well as the prior art) proved to be only conventional solid solutions with no congruent minimum.
- *Lattice parameter in the desired range*. Because of the goals of this study, the lattice parameters of the resultant perovskite solid solutions studied are those predicted to be near the region of interest 0.390 to 0.412 nm, particularly 0.400 to 0.411 nm, and most particularly 0.407 nm, which matches the average lattice parameter of lead zirconate titanate (PZT). In practical terms, a hypothetical $BaB^{4+}O_3$ compound with $t = 1$ would have B with a cation radius of 0.869 and a calculated lattice parameter of 0.4185 nm. Similarly, $SrB^{4+}O_3$ with $t = 1$ would have B with a cation radius of 0.749 and a calculated lattice parameter of 0.3918 nm. Therefore, the desired range provides some chemical constraints with the desired lattice parameter principally being available in solid solutions of Ba with a smaller ion. Practically, such smaller ions are Na and La. An optimum set of average cationic radii for $a = 0.407$ nm and $t = 1$ are IR(dod) = 0.1672 nm and IR(oct) = 0.08137 nm. For example, this condition would be satisfied by a La concentration of 0.312 atoms per formula unit in a Ba perovskite.
- *Similar melting temperatures*. As discussed further in the next paragraph, end member melting temperatures with a difference no greater than 300 °C were desired to keep the congruent composition sufficiently far away from the end members to be useful. In some cases, the end member melting temperatures had to be estimated.

For components with the same melting temperature and positive enthalpy of mixing, a first approximation is that either an indifferent point or a eutectic will be near the equimolar point in the center of the phase diagram. As the melting temperature difference increases, there is a tendency for the temperature minimum to move closer to the lower melting constituent. At a large enough difference, the minimum reaches the melting point of the end member constituent or is so close as not to have a significantly different set of properties from the end member. Empirically this tends to occur for differences in end-member melting temperatures ~ 400 °C. Therefore, initial estimates of the melting point T_m(est) and indifferent composition x_{est} were made based on the melting temperatures of the two components with initial assumptions that 1) the melting point depressions of both compounds were the same and given a value from the average of literature values and 2) the temperature difference where the melting minimum would reach the lower melting

Table 1
Properties of targeted end member compounds including: abbreviation used herein (Abb.), chemical formula, crystal structure (C.S.: cu = cubic, tet = tetragonal, o = orthorhombic, r = rhombohedral, h = hexagonal, and pc = pseudo-cubic where the exact crystal structure is undetermined), lattice parameters a, b, and c, pseudo-cubic lattice parameter a_{pc}, calculated hard-sphere lattice parameter a_{hs} (not adjusted for tolerance factor t or ionic size), tolerance factor t, melting temperature T_m and congruency (Cong: co = congruent, p = peritectic, sl = slightly incongruent, n = not congruent, and u = unknown). Starred melting temperatures and crystal structures are estimated.

Abb.	Formula	C.S.	a (nm)	b (nm)	c (nm)	a_{pc} (nm)	a_{hs} (nm)	t	T_m (°C)	Cong.
NN	$NaNbO_3$	o	0.5513	0.5571	0.7766	0.3907	0.4013	0.967	1425	co
NT	$NaTaO_3$	o	0.5481	0.5524	0.7795	0.3893	0.4013	0.967	1810	co
KN	$KNbO_3$	o	0.5695	0.5721	0.3974	0.4015	0.4190	1.054	1071	p
KT	$KTaO_3$	cu	0.3988			0.3988	0.4190	1.054	1368	p
CT	$CaTiO_3$	o	0.5404	0.5422	0.7651	0.3827	0.3942	0.966	1975	co
ST	$SrTiO_3$	cu	0.3903			0.3903	0.4013	1.002	2060	co
BT	$BaTiO_3$	tet	0.4000		0.4024	0.4008	0.4133	1.062	1625	co
LA	$LaAlO_3$	r	0.5359			0.3789	0.3887	1.009	2110	co
LG	$LaGaO_3$	o	0.5491	0.5523	0.7773	0.3892	0.3972	0.966	1698	co
LI	$LaInO_3$	o	0.5940	0.8216	0.5723	0.4118	0.4214	0.887	1825	co
SAN	$SrAl_{.5}Nb_{.5}O_3$	cu	0.7795			0.3898	0.3996	1.010	1790	co
SAT	$SrAl_{.5}Ta_{.5}O_3$	cu	0.7795			0.3898	0.3996	1.010	1980	co
SGT	$SrGa_{.5}Ta_{.5}O_3$	cu	0.7898			0.3949	0.4038	0.989	1820	co
BGN	$BaGa_{.5}Nb_{.5}O_3$	pc	0.4038			0.4038	0.4158	1.048	1500	sl
BGT	$BaGa_{.5}Ta_{.5}O_3$	pc	0.4038			0.4038	0.4158	1.048	1690	sl
BSN	$BaSc_{.5}Nb_{.5}O_3$	cu	0.4113			0.4113	0.4221	1.017	2130	co
NLT	$Na_{.5}La_{.5}TiO_3$	o	0.5479	0.5487	0.7747	0.3876	0.3967	0.979	1800*	u
KLT	$K_{.5}La_{.5}TiO_3$	pc	0.3914			0.3914	0.4056	1.023	1360	n
SLT	$SrLi_{.25}Ta_{.75}O_3$	r	0.9811	0.9811	1.1206	0.4005	0.4078	0.970	1905	co
SLN	$SrLi_{.25}Nb_{.75}O_3$	r*	0.9811	0.9811	1.1206	0.4005	0.4078	0.970	1635*	u
BLT	$BaLi_{.25}Ta_{.75}O_3$	h	0.5802	0.5802	1.9085	0.4112	0.4198	1.028	1620*	u
BLN	$BaLi_{.25}Nb_{.75}O_3$	h	0.5803	0.5803	1.9076	0.4112	0.4198	1.028	1350*	u
BNN	$BaNa_{.25}Nb_{.75}O_3$	c*	0.4146			0.4146	0.4263	0.997	1350*	u[a]
CNiN	$CaNi_{1/3}Nb_{2/3}O_3$	o	0.5473	0.5592	0.7796	0.3904	0.3994	0.942	1650	co
SNiN	$SrNi_{1/3}Nb_{2/3}O_3$	h	0.5649		0.6899	0.3991	0.4065	0.976	1875	n
BNiN	$BaNi_{1/3}Nb_{2/3}O_3$	h	0.5758		0.7052	0.4074	0.4113	1.035	1560*	u

[a] May contain anti-site Na on the A site.

temperature end member is 400 °C. Measured approximate values of the indifferent composition x_m and melting temperature T_m(meas), where determined, differ from these calculated values somewhat with x_m in particular being closer to the value where $t = 1$. In the one case where there is literature data for the indifferent composition x_{lit} and melting temperature T_m(lit), those data are tabulated as well, but they differ significantly from the current determination. It was assumed that any melting temperature difference greater than 300 °C would not give a congruent composition far enough away from lowest melting end member to be worth pursuing.

Table 1 contains a list of end member compounds tested or that are otherwise discussed.

Target solid-solution compounds were prepared in various proportions by pre-drying the constituents, initially reacting at 1000 °C, followed by repeated reactions at 1200 °C with intermediate grinding and pressing into a pellet. X-ray diffraction (XRD) was used to determine if the samples were single phase and, if not, the composition was adjusted until the resultant perovskite was single-phase cubic or determined to be a failure. A surprisingly large number of pairings were found to form solid solutions readily. Many were solid solutions with the well-known stable compounds barium titanate (BT) or strontium titanate (ST). All successful congruent solid solutions contained Na as one of the A-site ions.

All the starting chemicals are low to moderate cost and low toxicity. The compounds that failed did so through formation of second phases or completely different phases from the perovskites because of different combinations of the ions used. Eutectic behavior with separation into two end member perovskites was also observed in some failed pairs.

Samples from four of the successful series were melted both by optical float zone and simple melting in a platinum crucible in a furnace in air. In the latter case, the temperature was progressively raised until the recovered sample was found to have melted. Melting-point depression relative to both end members was measured in those four cases in Table 2. When slow cooled to room temperature, these compounds retained the desired cubic phase.

4. Results and discussion

Table 2 lists successful solid solution pairs that have been investigated to varying degrees.

Table 2
Successful solid solution pairs that form indifferent minimum points.

x	$(1-x)$	x_{est}	x_m (±0.1)	x_{lit}	t(est)	t	a (nm) (±1%)	T_m(est) (°C)	T_m(meas) (±100 °C)	T_m(lit) (°C)
BT	NN	0.25	0.32	0.5–0.6	0.990	0.997	0.3958	1362	1285	1290–1325
BT	NT	0.73	0.55		1.036	1.019	0.3962	1553	1440	
NN	BLN[a]	0.41	0.41		1.004	1.004	0.4110	1198	1300	
BT	NLT	0.72	0.35		1.038	1.008	0.3920	1547	1625	
ST	NT	0.19	0.40		0.974	0.981	0.3908	1772		
ST	NLT	0.18	0.25		0.983	0.984	0.3872	1766		
NN	BNiN	0.33			0.990	1.000[b]	0.4014	1320		

[a] May contain anti-site Na on B site substituting for Li.
[b] Only one composition tested at $t = 1.000$ and $x = 0.48$.

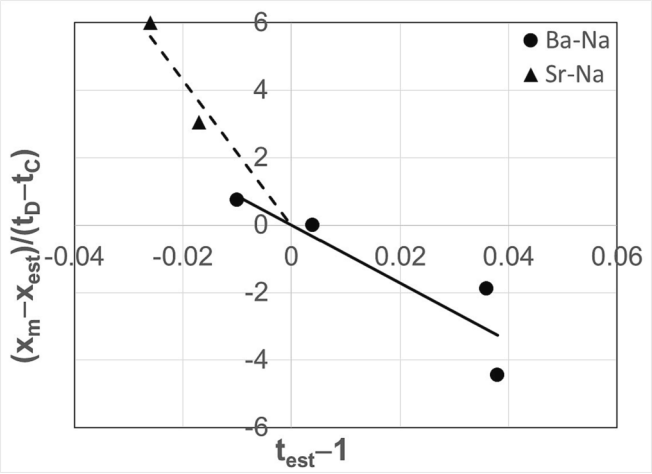

Fig. 8. $(x_m - x_{est})/(t_D - t_C)$ versus $(t_{est} - 1)$ for Ba-Na pairs (circles) and Sr-Na pairs (triangles) with possible trend lines forced through the origin. NN-BNiN is not plotted because x_m was not measured.

The tolerance factor at the actual indifferent point was, at worst, the same and mostly closer to unity than at the predicted indifferent point, suggesting that the tolerance factor has a thermodynamic influence on the energy minimum. A revised Eqn. would therefore be:

$$\Delta G_S = (1-x)\Delta G_C + x\Delta G_D + \Delta H_m + \Delta H_t - T\Delta S_m. \quad (8)$$

The functional form of the tolerance free energy contribution ΔH_t remains to be determined but it is assumed to be a function of the deviation from ideality $(t - 1)$. A crude estimate may be made from the deviations $x_m - x_{est}$ in Table 2. Differentiating Eqn. (8), solving for x, and subtracting Eqn. (6) yields:

$$x_m - x_{est} = 0.5(d\Delta H_t/dt \times dt/dx)/[H_{CD} - (H_{CC} + H_{DD})/2] \quad (8)$$

with $dt/dx = t_D - t_C$. Solving this for $d\Delta H_t/dt$ yields:

$$d\Delta H_t/dt = 2(x_m - x_{est})[H_{CD} - (H_{CC} + H_{DD})/2]/(t_D - t_C) \quad (9)$$

Fig. 8 shows the values of $(x_m - x_{est})/(t_D - t_C)$ plotted versus $(t_{est} - 1)$ for Ba-Na and Sr-Na A-site pairs. The two data sets are expected to have different enthalpy of mixing coefficients $[H_{CD} - (H_{CC} + H_{DD})/2]$ because of the different alkaline earth A-site ion and indeed this is seen in the different slopes. Within the data sets, some scatter is expected because of the varying enthalpies of mixing within the data sets owing to differences in composition on the B site and, in some cases, the addition of La on the A site.

Within those admittedly crude limits, the data is consistent with a linear relationship between $d\Delta H_t/dt$ and $(t_{est} - 1)$ with a zero intercept for each data set and a somewhat higher enthalpy of mixing slope for Sr-Na than Ba-Na. This suggests a quadratic functional form of $\Delta H_t = A(t - 1)^2$ with no first order term, where A is dependent on the ions used in ways that would require extensive additional modeling to derive. This is a more useful functional form than a linear dependence $\Delta H_t = A|(t - 1)|$, which requires an absolute value and therefore has a singularity in the derivative at $t = 1$ but a rigorous determination of the relation would require much more extensive research with a single variable in each data set.

BT—NN, BT—NT, and NN—BLN were more highly investigated and are discussed further below.

4.1. Barium Titanate—Sodium niobate solid solutions

A solid solution of barium titanate and sodium niobate was found with an approximate molar chemical formula of $x\text{BaTiO}_3$—$(1 - x)$ NaNbO_3 with $x \approx 0.32$, which grew polycrystalline with a uniform composition by float zone from a melt of the same chemical composition. The preferred growth range around the determined congruent composition is $x = 0.32 \pm 0.05$, where highest uniformity may be achieved. This compositional range is in direct contradiction of earlier publications. The perovskite tolerance factor $t = 0.997$ at the determined indifferent point is closer to the preferred value of unity than the

Table 3
X-ray powder diffraction pattern taken with a Siemens D-500 diffractometer for the $BT_{0.32}$—$NN_{0.68}$ cubic solid solution including inter-planar d-spacings, intensity percentage with respect to the maximum (1,1,0) line and planar (h,k, l) indices. The (1,1,1) and (3,1,1) lines have zero intensity, but are included because they have non-zero intensities for higher values of x in Table 4. The d spacings have an error bar of 2 %, and the intensities should not be considered as precise.

d(nm)	I%	(h,k,l)
0.3938	21 %	(1,0,0)
0.2789	100 %	(1,1,0)
	0 %	(1,1,1)
0.1975	41 %	(2,0,0)
0.1763	9 %	(2,1,0)
0.1616	25 %	(2,1,1)
0.1400	13 %	(2,2,0)
0.1252	10 %	(3,1,0)
	0 %	(3,1,1)
0.1142	6 %	(2,2,2)

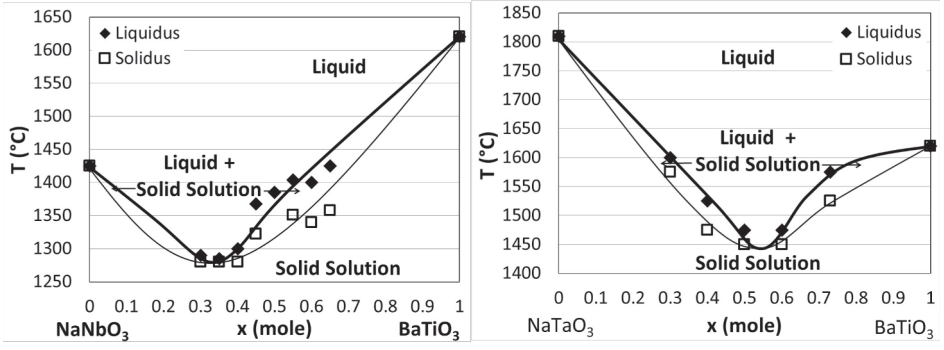

(a) (b)

Fig. 9. (a) Pseudo-binary phase diagram of the continuous solid solution $(1 - x)\text{NaNbO}_3$—$x\text{BaTiO}_3$ from the present work with an observed indifferent temperature minimum at $x \approx 0.32$. This result is in direct conflict with prior art Fig. 7a and 7b. The perovskite tolerance factor t is a preferred value of 0.997 nearly equal to unity. (b) Pseudo-binary phase diagram of the continuous solid solution $(1 - x)\text{NaTaO}_3$–$x\text{BaTiO}_3$ with an observed melting temperature minimum at $x \approx 0.55$ based on current experimental results. At this indifferent composition, the perovskite tolerance factor t is a value of 1.019 in the preferred range between 0.98 and 1.02.

Table 4
X-ray powder diffraction patterns for the xBT—$(1-x)$NN solid solutions for $x = 0.30$–0.65. Intensity percentage is with respect to the maximum (1,1,0) line. The BCC primitive unit cell lines (bold) have approximately constant intensity for all compositions, but (1,0,0)/(2,1,0) (italic) decrease with increasing x and (1,1,1)/(3,1,1) (regular font) decrease with increasing x.

(*h*,*k*,*l*)	0.30	0.35	0.40	0.45	0.50	0.55	0.60	0.65
(1,0,0)	*22 %*	*15 %*	*12 %*	*7 %*	*3 %*	*4 %*	*2 %*	*2 %*
(1,1,0)	**100 %**	**100 %**	**100 %**	**100 %**	**100 %**	**100 %**	**100 %**	**100 %**
(1,1,1)	0 %	0 %	4 %	5 %	7 %	10 %	11 %	13 %
(2,0,0)	**45 %**	**42 %**	**42 %**	**50 %**	**40 %**	**47 %**	**39 %**	**42 %**
(2,1,0)	*7 %*	*5 %*	*3 %*	*0 %*	*0 %*	*0 %*	*0 %*	*0 %*
(2,1,1)	**32 %**	**34 %**	**36 %**	**45 %**	**36 %**	**47 %**	**39 %**	**45 %**
(2,2,0)	**13 %**	**21 %**	**18 %**	**23 %**	**21 %**	**25 %**	**21 %**	**21 %**
(3,1,0)	**10 %**	**9 %**	**12 %**	**10 %**	**14 %**	**15 %**	**12 %**	**17 %**
(3,1,1)	0 %	0 %	0 %	0 %	0.2 %	3 %	3 %	2 %
(2,2,2)	**3 %**	**5 %**	**5 %**	**5 %**	**5 %**	**7 %**	**6 %**	**6 %**

compositions previously published. Fig. 9a displays the congruent melting behavior observed in the current study and may be contrasted with Fig. 7a,b.

The structure remains cubic at room temperature for all samples measured for $x = 0.3$–0.65, and the range may prove broader with additional measurements. The $x = 0.32$ compound $BT_{0.32}$—$NN_{0.68}$ has a simple perovskite lattice parameter of approximately 0.3958 nm and indexes to a simple perovskite cubic cell with two additional lines (1,0,0) and (2,1,0) (see Table 3). Table 4 shows that there is more complexity to the x-ray pattern as it is examined across the phase diagram.

The (1,0,0), (1,1,1), (2,1,0), and (3,1,1) lines would not appear if the solid solution was fully disordered with a primitive unit cell. The (1,0,0) and (2,1,0) lines become more intense at lower x near the indifferent point, while the (1,1,1) and (3,1,1) lines decrease and disappear. Ordering can appear during cooling, but since these samples were furnace quenched, the fictive (equilibrium) temperature is high. This could indicate that an ordering transition, probably second order, is responsible for the difference in the two phases on either side of the minimum, therefore satisfying the simplified phase rule, though as discussed above, this is not necessary. This could result from partial ordering or clustering resulting from the positive enthalpy of mixing. It could also be a consequence of the differing x–ray cross sections of the substituting ions, particularly between Ba and Na. More-detailed investigative methods (including electron microscopy and spectroscopic techniques) would be required to understand this better.

Cryoscopic examination of a melted charge of $0.32BaTiO_3$—$0.68NaNbO_3$ returned to room temperature did not reveal the lamellar structure typical of eutectic crystallization.

This material would be a valuable substrate for lattice-matched $BiFeO_3$, which is currently grown with highest perfection on $DyScO_3$[13,14] and $TbScO_3$[15], substrates of high cost, limited size, and limited availability, but with a very good stability at high temperatures.

4.2. Barium Titanate—Sodium tantalate solid solutions

A perovskite comprising a similar solid solution of the compounds barium titanate and sodium tantalate with an approximate molar chemical formula of $x BaTiO_3$—$(1-x)NaTaO_3$ with $x \approx 0.55$, yielded crystals from a melted charge of the same chemical composition. The preferred growth range is immediately adjacent to the congruent composition $x = 0.55 \pm 0.05$, where highest uniformity may be achieved. Ta is chemically similar to Nb and has the same ionic size. The tantalates are more refractory with melting temperatures 300–400 °C higher for the end members, which would tend to push the indifferent point toward the BT side of the phase diagram. On the other hand, the tolerance factor contribution to free energy pushes the minimum back toward the center as seen in Fig. 9b.

Based on melting temperatures alone, the estimated indifferent point would be $x = 0.73$ where the calculated tolerance factor would be $t = 1.036$, while the measured melting minimum is at $x = 0.55$ where the calculated tolerance factor is $t = 1.019$. This is halfway between the melting temperature estimate of the indifferent point and the solid solution composition where $t = 1.000$, which is $x = 0.35$.

Visually the NN—BT phase diagram appears congruent, but the NT—BT phase diagram appears sharper, which could indicate a eutectic. Nevertheless, no phase separation was seen in recovered charges. In this study, some compounds grow more readily as niobates and some as tantalates.

4.3. Sodium Niobate—Barium lithium niobate solid solutions

Examples of the $AE^{2+}Alk^{1+}_{0.25}B^{5+}_{0.75}O_3$ class of compounds were reported by Galasso and Pinto [16] with AE = Ba, Alk = Na and B = Nb and Ta. Experience has shown that Na distorts the B site and therefore the structure. Li is of a more reasonable size but requires a large A site ion. The compound SLT ($SrLi_{0.25}Ta_{0.75}O_3$), was previously found to be congruently melting[17], but was unfortunately slightly off cubic with a destructive phase transition. This likely results from the size discrepancy between Sr and Li relative to their sites. The niobium cognate, SLN ($SrLi_{0.25}Nb_{0.75}O_3$), had issues of reduction of the niobium, which darkened the crystal in spite of the lower melting temperature and made further investigation impractical. The barium cognates have $t = 1.028$ so a near equimolar solid solution between NN and BLN would have $t \sim 1$ with the Ba alleviating the stress and incompatibility seen previously between the ionic sizes of Li and Sr. Furthermore, although these compounds have not had their melting temperatures determined, Ba-containing compounds generally have lower melting points than the equivalent Sr compounds (e. g. BaO 1923 °C/SrO 2531 °C, $BaTiO_3$ 1625 °C/$SrTiO_3$ 2080 °C and $Ba_2GaNbO_6 \sim 1500$ °C [18]/Sr_2GaNbO_6 1720 °C [19]). A congruently melting minimum will lower this still further. This can eliminate issues of reduction seen at higher temperatures. Recent results suggest that $BaNa_{0.25}Nb_{0.75}O_3$ (BNN) may have a more complex position in the BaO-Na_2O-Nb_2O_5 ternary phase diagram with Na occurring on both the A and B sites and the overall composition adjusted to meet stoichiometry requirements. This, unfortunately, creates another degree of freedom.

The solid solution between $NaNbO_3$ (NN) and $BaLi_{0.25}Nb_{0.75}O_3$ (BLN) was investigated at a variety of proportions by powder reaction and the composition with a single-phase cubic structure indicative of congruency had a lattice parameter higher than predicted. This lattice parameter is positioned in the gap in the substrate lattice parameter line and the material could be uniquely valuable as a substrate for lattice-matched piezoelectric materials such as $Pb(Zr,Ti)O_3$ (PZT) and $BiScO_3$, which are now commonly grown on poorly matched strontium titanate substrates [20–24] or $SrTiO_3$-buffered silicon substrates [25–27]. Further, such a lattice constant would be appropriate for the perovskite semiconductor $BaSnO_3$, which shows promise for transparent transistors [28] due to its 3.1 eV bandgap [29] and room-temperature mobility of

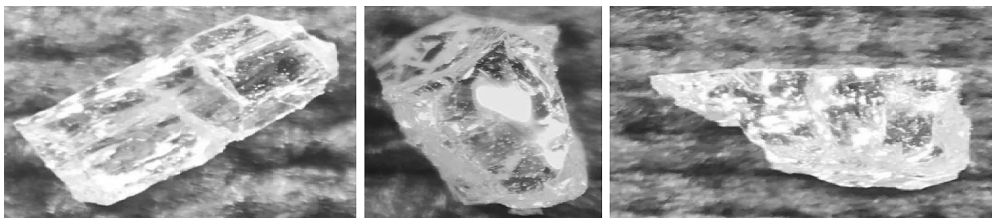

Fig. 10. Small pieces of a broken $0.41NaNbO_3$—$0.59BaLi_{0.25}Nb_{0.75}O_3$ crystal 1–3 mm on a side extracted from a Bridgman crucible.

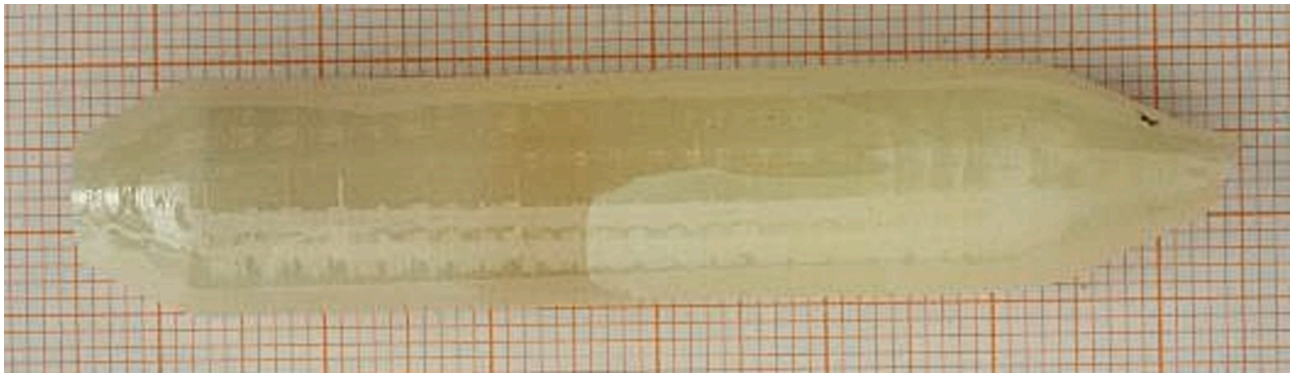

Fig. 11. Initial Czochralski boule grown from the NN—BLN system. Three separate crystals can be seen along with clear and cloudy areas. The cloudiness likely results from a second phase.

320 $cm^2\ V^{-1}\ s^{-1}$ in single crystals [30] and 183 $cm^2\ V^{-1}\ s^{-1}$ in thin films [31]. The lower mobility in films is ascribed in part to the large density ($\sim 10^{11}\ cm^{-2}$) of threading dislocations[31]. A lattice-matched substrate would reduce or eliminate these threading dislocations. Accordingly, an NN—BLN single-crystal substrate could be of high technological use.

A melting curve was not determined, but the apparently congruent sample melted at the low temperature of ~ 1300 °C, and cryoscopic examination of the melted charge of $0.41NaNbO_3$—$0.59BaLi_{0.25}Nb_{0.75}O_3$ returned to room temperature did not reveal the lamellar structure typical of eutectic crystallization. The low cost of ingredients and the low melting temperature make this material very technologically accessible.

Recently Bridgman growth of this compound was attempted from a crucible made from a platinum tube with the ends pinched. Issues of reactivity of the charge with the platinum crucible were seen and a hole occurred in the crucible during the growth run. Sodium oxide may have decomposed creating sodium vapor. While such evaporation occurred previously in powder samples, it was not contained and concentrated, thus having no effect. In this case, the closed crucible may have caused the reaction of sodium vapor with platinum to form a low melting temperature alloy that melted and further caused recrystallization and formation of domain walls in the area that was in contact with the charge. An open crucible, oxygen over-pressure, or an alloy crucible may be required to ameliorate this.

Crystals were seen in the bottom of the crucible. The charge broke up as the crucible was removed and the full size of the as-grown crystals is not known. Pictures of broken pieces removed are shown in Fig. 10. It is notable that the crystals are water white with no Nb reduction apparent.

The lattice parameter of one of these single crystal samples was measured to be 0.411 nm, which is larger than expected. These results suggest that the NN—BLN indifferent composition may have Na occurring on both the A and B sites with Na substituting for Li.

The first Czochralski run at IKZ in Berlin (unseeded—Fig. 11) produced a well-formed boule ~ 14 mm in diameter with three separate crystals and some cloudy areas. The lattice parameter was still higher a = 0.4138 nm tending to confirm the presence of Na on the octahedral site. The target congruent composition has been revised accordingly. Unfortunately, safety concerns that will be discussed below have halted this work.

4.4. Sodium evaporation

As shown in Fig. 12a, it is well known that at high temperatures sodium carbonate decomposes to sodium oxide and at still higher temperatures, it decomposes to Na vapor and oxygen. (Potassium is even worse in this regard.) As oxygen is added, this tendency is significantly reduced by a factor of approximately three, but not eliminated. A pure oxygen atmosphere presents safety hazards of promoting combustion at high temperatures of various substances that may be in the growth chamber.

Carbon dioxide (CO_2) can also increase the oxygen activity in the chamber, but not as effectively as pure O_2. A blend of 80 % CO_2-20 % O_2, is therefore more effective than a similar Ar-O_2 blend, but safer than pure O_2. Interestingly, Fig. 12b shows that it is also more effective by a factor of two at suppressing Na evaporation than either pure CO_2 or pure O_2 (the actual minimum is about 60 % CO_2-40 % O_2) at 1600 °C. At 1350 °C, this change in atmosphere is expected to be even more effective.

Sodium vapor in the system is expected to condense out on cooler portions of the furnace. In Czochralski growth, this included the seed holder made of Pt-Rh wire. The wire then experienced alloying, recrystallization, and embrittlement like the Bridgman crucible. This resulted in the wire breaking and dropping the seed. In addition, the vapor condensing on other portions of the furnace reacts with the ambient atmosphere during growth if the surface is cool enough or on cooling. In the 80 % Ar-20 % O_2 used for the previous growth runs, this results in formation of Na_2O powder. On opening of the chamber, this powder became airborne and flew out of the chamber, then reacted quickly with external ambient water/water vapor to form NaOH, which is highly corrosive. In one incident, this material was inhaled by an operator with consequent significant health issues.

Such hazardous reactive species must be avoided at all costs. The 80 % CO_2-20 % O_2 atmosphere presents a significant advantage in this regard. Below approximately 500 °C sodium carbonate will form from either Na or Na_2O. This is a slower reaction than the sodium hydroxide formation, but if the chamber is under a predominantly CO_2 atmosphere with no water vapor during growth and cooldown, there should be ample time for the carbonate reaction to occur. Sodium carbonate is a

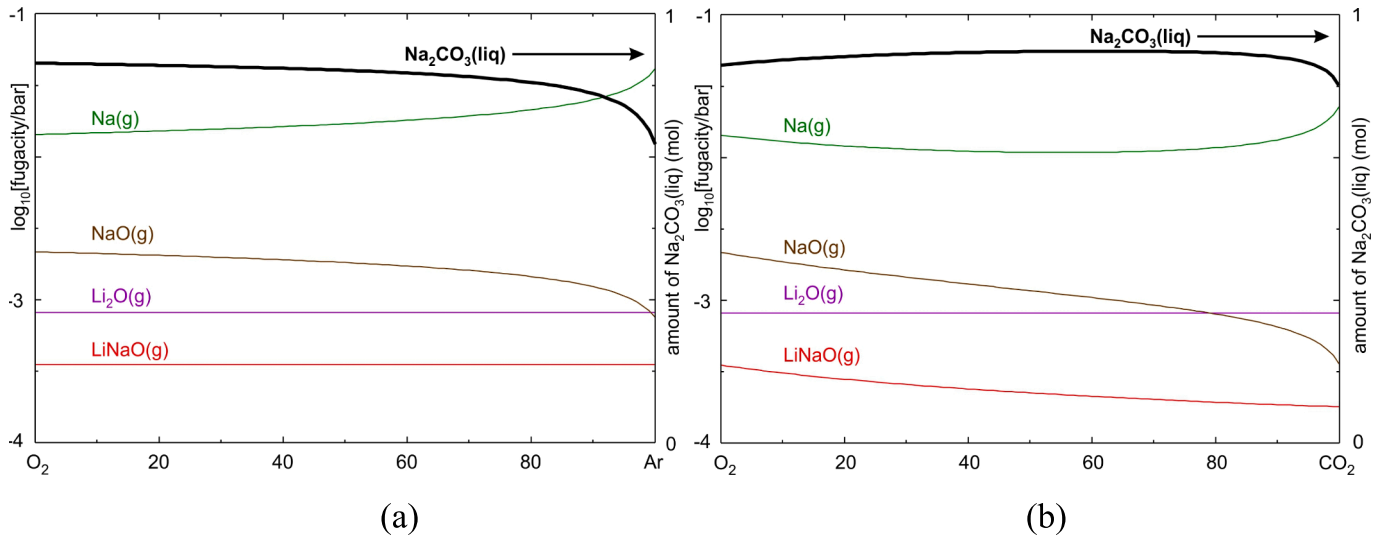

Fig. 12. Fugacities (logarithmic scale) for main species when a mixture of 1 mol Na_2CO_3, 3 mol $BaCO_3$, 0.375 mol Li_2CO_3, and 2.125 mol Nb_2O_5 is heated to 1600 °C in different atmospheres (10 mol gas in total). (a) Mixtures between O_2 (left) and Ar (right), (b) Mixtures between O_2 (left) and CO_2 (right). The dark black curve (right linear ordinate) shows the total amount of liquid Na_2CO_3 that remains in the melt.

much safer and more inert substance even in powder form, though inhalation and eye/skin contact should still be prevented with proper use of personal protective equipment. Therefore, it is hoped that an 80 % CO_2-20 % O_2 growth and cooling atmosphere will stabilize the growth and passivate any evaporation products for much improved safety. This remains to be proven in practice. Proper exhausting of the system will still be important to remove CO_2 from the ambient atmosphere in the laboratory. Because all the compounds in Table 2 contain sodium, these measures will be necessary for all the compounds of this class discovered in this study. At present, the use of sodium is considered too hazardous for the available facility.

4.5. BT ($BaTiO_3$) —NLT ($Na_{0.5}La_{0.5}TiO_3$)

Naturally occurring loparite is a mixture of a variety of elements, but synthetics are generally $Na_{0.5}Ln_{0.5}TiO_3$, where Ln is a large lanthanide, La, Ce, Pr, or Nd. $Na_{0.5}La_{0.5}TiO_3$ has a tolerance factor $t = 0.979$ that is offset by the higher tolerance factor of BT ($t = 1.062$) in this solid solution. This resulted in a large shift from the predicted congruent composition of $x = 0.72$ ($t = 1.038$) based on end member melting to an observed single-phase cubic composition of $x = 0.35$ ($t = 1.008$). This is the largest such shift of any of the mixtures that were fully investigated in powder form. Roy found $K_{0.5}La_{0.5}TiO_3$ ($t = 1.023$) melted incongruently, but $K_{0.5}Ce_{0.5}TiO_3$ ($t = 0.984$–1.019, depending on Ce valence) melted congruently.[32] Compared to other rare earths, La is readily available and inexpensive.

4.6. Strontium-Containing solid solutions

The strontium-containing samples were investigated across a range of compositions to find a single-phase cubic composition. Unfortunately, their high melting temperatures coupled with the high vapor pressure of sodium made further investigation ineffective without a sealed crucible in a high-temperature furnace and no melting was attempted.

4.7. Nickel-Containing solid solutions

Nickel containing compounds were identified late in the process based on previous work[33] on nickel-containing perovskites. Using the tolerance factor contribution to congruency, three nickel-containing solid solutions NN—BNiN, SNiN—BNiN, and CNiN—BNiN were hypothesized, and single samples were prepared by conventional powder reaction techniques at a composition that yields a tolerance factor $t = 1.000$. NN—BNiN and SNiN—BNiN were single-phase cubic perovskite solid solutions as reacted, but the CNiN—BNiN sample phase separated completely into the two component phases, likely because of the ionic radius difference of the alkaline earths. The solid solution 0.4SNiN—0.6BNiN was single phase and had a lattice parameter of 0.4013 nm. Additional study suggests, however, that because of Ba and Sr being too similar in size and valence, this is a simple solid solution with no or insufficient positive heat of mixing to create an indifferent point as seen in other systems. So only NN—BNiN is listed in Table 2. Ni-containing compounds may be limited in use because of nickel's magnetic properties and higher vapor pressure. These samples were not melted.

4.8. Lanthanum-containing solid solutions

As mentioned above, lanthanum is the best logical alternative for a lower ionic radius A-site ion, but early experiments in this study with lanthanum aluminate (LA) and lanthanum gallate (LG) were unsuccessful and were also low in projected lattice parameter. Work with $BaTiO_3$—$LaInO_3$ solid solutions seems promising, but In_2O_3 has issues in that it decomposes and evaporates beginning at 850 °C. Nonetheless, if pre-reacted thoroughly, this does not seem to be as much of an issue from compounds containing indium.

4.9. Generalizations

There is a much higher level of complexity in a xABO$_3$—$(1 - x)$ A′B′O$_3$ solid solution than in the simple C—D example depicted in Fig. 5b. The various functional forms therefore allow an even higher number of free energy phase diagrams than are shown in this study. Enhancements to the simplistic procedure described in this manuscript would be to make refinements based on the following corrections or existing work.

- The entropy of mixing of the liquid will be inherently higher than the solid because of the site constraints of all three types of ions in the solid and the possibilities of oxide dissociation and multiple types of cation species with various oxygen coordinations in the melt. This changes the entropy's functional form and curve shape.
- The enthalpy of mixing of the solid will depend on nearest and next-nearest neighbors among the A- and B-sites. Ordering could be some

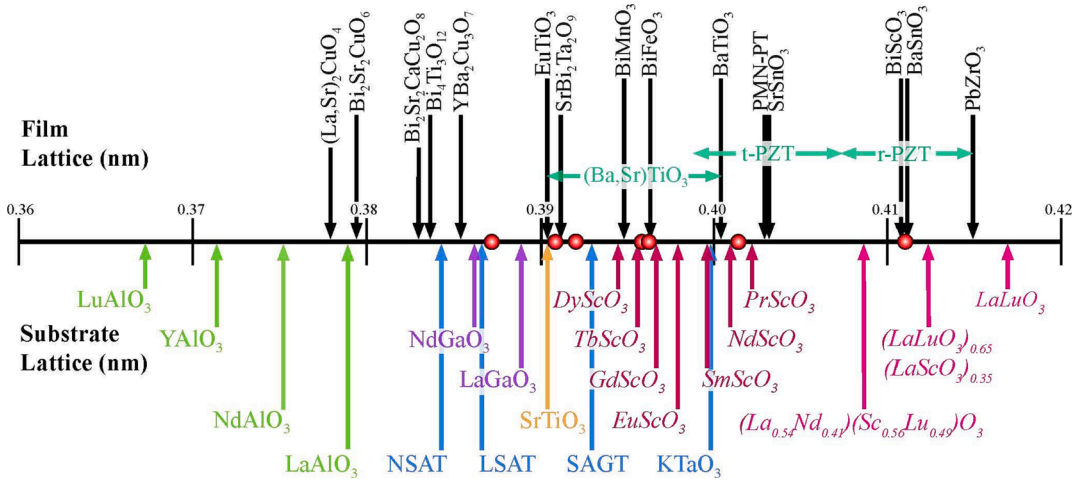

Fig. 13. New compositions shown as red circles on the lattice parameter number line. (For interpretation of the references to colour in this figure legend, the reader is referred to the web version of this article.)

form of alternating or discrete clustering. Electron microscopy and spectroscopy would be useful tools to determine preferred arrangements.

- The tolerance factor t contributes a free energy that is at a minimum for $t = 1.00$. This will reinforce the entropy of mixing in the solid solution and can counteract an excess of positive enthalpy of mixing to eliminate phase separation. It will have a different functional form than any of the other free energies and is not completely understood. Thermodynamic measurements are required.
- The constraint formalism of Tidrow[34] could potentially be used with computer modeling to determine the lowest-energy ordering on the various sites based on a combination of packing, stress, and electrostatic energies. The use of t is a simplified metric for packing efficiency in two and three dimensions. Tidrow[34] has further amplified on this. This term can, in some cases, provide a singular solution that permits an indifferent point and effectively removes one degree of freedom.
- Lufaso, Barnes, and Woodward [35] have used a well-tested approach based on the bond valence concept to predict structures of complex perovskites, including Glazer tilt. The authors have developed user-friendly software called "SpuDS."[36]
- Other oxide systems do not have such a simplified formalism but may also have solid solutions that are congruently melting. Substituted rare-earth garnets provide multiple examples. The rare-earth scandium gallium garnets (RESGG) would have a simple formula of $RE_3Sc_2Ga_3O_{12}$ if the lowest room temperature free energy sites were observed. In fact, the congruent composition of gadolinium scandium gallium garnet (GSGG) is $Gd_{2.957}Sc_{1.905}Ga_{3.138}O_{12}$ or, given by site occupancies, $\{Gd_{2.957}Sc_{0.043}\}[Sc_{1.862}Ga_{0.138}](Ga)O_{12}$ where {} denotes the dodecahedral site, [] denotes the octahedral site, and () denotes the tetrahedral site.[37] These off-site distributions may be viewed as a solid solution among end members consisting of real stoichiometric compounds GSGG and GGG (gadolinium gallium garnet, which also has anti-site Ga) and an imaginary extrapolated compound (e.g., $Sc_3Ga_2Ga_3O_{12}$). Mateika and co-workers found congruent or near-congruent compositions by putting paired "guest ions" such as $REAlO_3$ in perovskites [7] and various pairs in garnets [38].

A higher understanding of all these factors is needed for a full characterization of the empirically determined compositions of the apparent indifferent point.

5. Conclusion

Perovskite solid solutions were investigated to identify compounds that have indifferent melting minima and cubic crystal structure with favorable lattice constants in the range 0.390–0.412 nm. Solid solution pairs that form indifferent points include, but are not limited to, seven compositions identified in this study. The lattice parameters of the new materials are plotted on the number line in Fig. 13 and show a broad range of desirable lattice constants. A perovskite tolerance factor close to unity was found to give a favorable contribution to the free energy so that these compositions tended toward $t = 1.00$ and consequently were more likely to have a cubic crystal structure. These constitute a broad and important class of compounds not previously anticipated. The constituents are inexpensive and non-toxic and many of the compositions have low melting points. The only significant drawback is the high vapor pressure of sodium, which is present in most of these materials. Given this number of successes, it is anticipated that a full mapping of all perovskite solid solutions would yield a significant additional number of perovskite solid solutions with indifferent congruently melting compositions at temperature minima of their respective melting curves.

CRediT authorship contribution statement

Vincent J. Fratello: Conceptualization, Data curation, Formal analysis, Funding acquisition, Investigation, Methodology, Project administration, Resources, Software, Supervision, Validation, Visualization, Writing – original draft, Writing – review & editing. **Lynn A. Boatner:** Investigation, Writing – original draft. **Hanna A. Dabkowska:** Investigation. **Antoni Dabkowski:** Investigation, Writing – original draft. **Theo Siegrist:** Investigation, Funding acquisition. **Kaya Wei:** Investigation. **Christo Guguschev:** Investigation, Methodology, Writing – original draft. **Detlef Klimm:** Conceptualization, Investigation, Methodology, Visualization. **Mario Brützam:** Investigation. **Darrell G. Schlom:** Investigation, Writing – original draft. **Shanthi Subramanian:** Investigation.

Declaration of competing interest

The authors declare the following financial interests/personal relationships which may be considered as potential competing interests: [The author V.J.F. was granted US Patent # 10,378,123 B2 (13 August 2019) with the title "Single-crystal perovskite solid solutions with indifferent points for epitaxial growth of single crystals."].

Data availability

Data will be made available on request.

Acknowledgements

The work by K.W. and T.S. was carried out at the National High Magnetic Field Laboratory, which is supported by the National Science Foundation (DMR-2128556) and the State of Florida.

References

[1] L.W. Martin, D.G. Schlom, Advanced Synthesis Techniques and Routes to New Single-Phase Multiferroics, Current Opinion in Solid State and Materials Science 16 (2012) 199, https://doi.org/10.1016/j.cossms.2012.03.001.
[2] F.A. Hummel, Introduction to Phase Equilibria in Ceramic Systems, Marcel Dekker Inc, New York, 1984, p. 86.
[3] M. Feinberg, On Gibbs' Phase Rule, Archive for Rational Mechanics and Analysis 70 (1979) 219, https://doi.org/10.1007/BF00280534.
[4] P.P. Fedorov, "Compositions of Congruently Melting Three-Component Solid Solutions Determined by Finding Acnodes on Ternary-System Fusion Surfaces," in Growth of Crystals Volume 20 ed. by E. I. Givargizov and A. M. Melnikova, translated by Dennis W. Wester (Consultants Bureau, New York, 1996).
[5] J.W. Tester, M. Modell, Thermodynamics and Its Applications, 3rd edition, Prentice Hall, Upper Saddle River, NJ, 1997.
[6] C. Kuper, R. Pankrath, H. Hesse, Appl. Phys. a: Mater. Sci. Process. A65 (1997) 301), https://doi.org/10.1007/s003390050583.
[7] D. Mateika, H. Kohler, H. Laudan, E. Völkel, Mixed-Perovskite Substrates for High-Tc Superconductors, J. Cryst. Growth 109 (1991) 449, https://doi.org/10.1016/0022-0248(91)90215-Q.
[8] M. Berkowski, R. Aleksiyko, J. Fink-Finowicki, R. Diduszko, P. Byszewski, R. Kikalejshvili-Domukhovska, Growth and Structure of $SrAl_{0.5}Ta_{0.5}O_3$: $LaAlO_3$: $CaAl_{0.5}Ta_{0.5}O_3$ Solid Solutions Single Crystals, J. Cryst. Growth 269 (2004) 512, https://doi.org/10.1016/j.jcrysgro.2004.05.100.
[9] V.M. Goldschmidt, "Geochemische Verteilungsgesetze der Elemente", Skrifter Norske Videnskaps – Akad, Oslo, (i) Mat. Naturv. Kl. No. 2 (1926).
[10] R.D. Shannon, Revised Effective Ionic Radii and Systematic Studies of Interatomic Distances in Halides and Chalcogenides, Acta. Cryst. A32 (1976) 751, https://doi.org/10.1107/S0567739476001551.
[11] D.E. Rase and R. Roy, ACerS-NIST Ceramic Phase Equilibria Diagrams, Version 4.0, American Ceramic Society and National Institute of Standards and Technology, (2014), Phase Diagram 00826 originally from Eighth Quarterly Progress Report (April 1 to June 30, 1953), Vol. Appendix II, p. 16 (1953).
[12] M.W. Schaefer, Phase Equilibria in the Na_2O-Nb_2O_5 and $NaNbO_3$-$BaTiO_3$ Systems, and the Polymorphism of $NaNbO_3$ and Nb_2O_5, Ph.D. thesis, The Pennsylvania State University (August, 1956)).
[13] J.F. Ihlefeld, W. Tian, Z.K. Liu, W.A. Doolittle, M. Bernhagen, P. Reiche, R. Uecker, R. Ramesh, D.G. Schlom, Adsorption-Controlled Growth of $BiFeO_3$ by MBE and Integration with Wide Band Gap Semiconductors, IEEE Transactions on Ultrasonics, Ferroelectrics, and Frequency Control 56 (2009) 1528–1533, https://doi.org/10.1109/ISAF.2008.4693774.
[14] A.B. Mei, Y. Tang, J. Schubert, D. Jena, H.G. Xing, D.C. Ralph, D.G. Schlom, Self-Assembly and Properties of Domain Walls in $BiFeO_3$ Layers Grown via Molecular-Beam Epitaxy, APL Mater. 7 (2019) 071101, https://doi.org/10.1063/1.5103244.
[15] C.T. Nelson, B. Winchester, Y. Zhang, S.-J. Kim, A. Melville, C. Adamo, C. M. Folkman, S.-H. Baek, C.B. Eom, D.G. Schlom, L.Q. Chen, X.Q. Pan, Spontaneous Vortex Nanodomain Arrays at Ferroelectric Heterointerfaces, Nano Lett. 11 (2011) 828–834, https://doi.org/10.1021/nl1041808.
[16] F. Galasso, J. Pinto, Preparation of $Ba(Na_{0.25}Ta_{0.75})O_3$ and $Sr(Na_{0.25}Ta_{0.75})O_3$ with the Perovskite Structure, Inorg. Chem. 4 (1965) 255, https://doi.org/10.1021/ic50024a033.
[17] V.J. Fratello, G.W. Berkstresser, A.J. Ven Graitis and I. Mnushkina, "A New Perovskite Substrate Material, Strontium Lithium Tantalate", invited talk presented at the 14th International Conference on Crystal Growth, Grenoble, France, August 9-13, 2004.
[18] V.J. Fratello, G.W. Berkstresser, C.D. Brandle, A.J. Ven Graitis, A.J. Valentino, Pyrochlore and Perovskite Compositions as Possible Substrates for High Temperature Superconductors, in, ACCG/east-95 Eastern Regional Conference on Crystal Growth, Atlantic City, NJ, October 15-18, 1995 (unpublished), 1995.
[19] C.D. Brandle, V.J. Fratello, Preparation of perovskite oxides for high Tc superconductor substrates, J. Mater. Res. 5 (1990) 2160, https://doi.org/10.1557/JMR.1990.2160.
[20] C.B. Eom, R.B. van Dover, J.M. Phillips, D.J. Werder, J.H. Marshall, C.H. Chen, R. J. Cava, R.M. Fleming, D.K. Fork, Fabrication and Properties of Epitaxial Ferroelectric Heterostructures with ($SrRuO_3$) Isotropic Metallic Oxide Electrodes, Appl. Phys. Lett. 63 (1993) 2570–2572, https://doi.org/10.1063/1.110436.
[21] M. de Keijser, J.F.M. Cillessen, R.B.F. Janssen, A.E.M.D. Veirman, D.M. de Leeuw, Structural and Electrical Characterization of Heteroepitaxial Lead Zirconate Titanate Thin Films, J. Appl. Phys. 79 (1996) 393–402, https://doi.org/10.1063/1.360843.
[22] J.H. Kim, A.T. Chien, F.F. Lange, L. Wills, Microstructural and Ferroelectric Properties of a Chemical Solution Deposited Epitaxial $PbZr_{0.5}$ $Ti_{0.5}O_3$ Thin Film on a $SrRuO_3$/$SrTiO_3$ Substrate, J. Mater. Res. 14 (1999) 1190–1193, https://doi.org/10.1557/JMR.1999.0160.
[23] I. Vrejoiu, G.L. Rhun, L. Pintilie, D. Hesse, M. Alexe, U. Gösele, Intrinsic Ferroelectric Properties of Strained Tetragonal $PbZr_{0.2}Ti_{0.8}O_3$ Obtained on Layer–by–Layer Grown, Defect-Free Single–Crystalline Films, Adv. Mater. 18 (2006) 1657–1661, https://doi.org/10.1002/adma.200502711.
[24] S. Trolier-McKinstry, M.D. Biegalski, J. Wang, A.A. Belik, E. Takayama-Muromachi, I. Levin, Growth, Crystal Structure, and Properties of Epitaxial $BiScO_3$ Thin Films, J. Appl. Phys. 104 (2008) 044102, https://doi.org/10.1063/1.2964087.
[25] B.T. Liu, K. Maki, Y. So, V. Nagarajan, R. Ramesh, J. Lettieri, J.H. Haeni, D. G. Schlom, W. Tian, X.Q. Pan, F.J. Walker, R.A. McKee, Epitaxial La–doped $SrTiO_3$ on Silicon: A Conductive Template for Epitaxial Ferroelectrics on Silicon, Appl. Phys. Lett. 80 (2002) 4801–4803, https://doi.org/10.1063/1.1484552.
[26] D.M. Kim, C.B. Eom, V. Nagarajan, J. Ouyang, R. Ramesh, V. Vaithyanathan, D. G. Schlom, Thickness Dependence of Structural and Piezoelectric Properties of Epitaxial $Pb(Zr_{0.52}Ti_{0.48})O_3$ Films on Si and $SrTiO_3$ Substrates, Appl. Phys. Lett. 88 (2006) 142904, https://doi.org/10.1063/1.2185614.
[27] S.H. Baek, J. Park, D.M. Kim, V.A. Aksyuk, R.R. Das, S.D. Bu, D.A. Felker, J. Lettieri, V. Vaithyanathan, S.S.N. Bharadwaja, N. Bassiri-Gharb, Y.B. Chen, H. P. Sun, C.M. Folkman, H.W. Jang, D.J. Kreft, S.K. Streiffer, R. Ramesh, X.Q. Pan, S. Trolier-McKinstry, D.G. Schlom, M.S. Rzchowski, R.H. Blick, C.B. Eom, Giant Piezoelectricity on Si for Hyperactive MEMS, Science 334 (2011) 958–961, https://doi.org/10.1126/science.120718.
[28] J. Park, H. Paik, K. Nomoto, K. Lee, B.-E. Park, B. Grisafe, L.-C. Wang, S. Salahuddin, S. Datta, Y. Kim, D. Jena, H.G. Xing, D.G. Schlom, Fully Transparent Field-Effect Transistor with High Drain Current and On-Off Ratio, APL Mater. 8 (2020) 011110, https://doi.org/10.1063/1.5133745.
[29] H. Mizoguchi, H.W. Eng, P.M. Woodward, Probing the Electronic Structures of Ternary Perovskite and Pyrochlore Oxides Containing Sn^{4+} or Sb^{5+}, Inorg. Chem. 43 (2004) 1667–1680, https://doi.org/10.1021/ic034551c.
[30] H.J. Kim, U. Kim, H.M. Kim, T.H. Kim, H.S. Mun, B.-G. Jeon, K.T. Hong, W.-J. Lee, C. Ju, K.H. Kim, K. Char, High Mobility in a Stable Transparent Perovskite Oxide, Appl. Phys. Express 5 (2012) 061102, https://doi.org/10.1143/APEX.5.061102.
[31] H. Paik, Z. Chen, E. Lochocki, A.H. Seidner, A. Verma, N. Tanen, J. Park, M. Uchida, S.L. Shang, B.-C. Zhou, M. Brützam, R. Uecker, Z.K. Liu, D. Jena, K. M. Shen, D.A. Muller, D.G. Schlom, Adsorption-Controlled Growth of La-doped $BaSnO_3$ by Molecular-Beam Epitaxy, APL Mater. 5 (2017) 116107, https://doi.org/10.1063/1.5001839.
[32] R. Roy, Multiple Ion Substitution in the Perovskite Lattice, J. Amer. Ceram. Soc. 37 (1954) 581, https://doi.org/10.1111/j.1151-2916.1954.tb13992.x.
[33] V.J. Fratello, G.W. Berkstresser, C.D. Brandle, A.J. Ven Graitis, Nickel Containing Perovskites, J. Cryst. Growth 166 (1996) 878, https://doi.org/10.1016/0022-0248(95)00474-2.
[34] S.C. Tidrow, Mapping Comparison of Goldschmidt's Tolerance Factor with Perovskite Structural Conditions, Ferroelectrics 470 (2014) 13, https://doi.org/10.1080/00150193.2014.922372.
[35] M.W. Lufaso, P.W. Barnes, P.M. Woodward, Structure prediction of ordered and disordered multiple octahedral cation perovskites using SPuDS, Acta Cryst. B62 (2006) 397, https://doi.org/10.1107/S010876810600262X.
[36] https://lufaso.domains.unf.edu/spuds/index.html.
[37] V.J. Fratello, C.D. Brandle, A.J. Valentino, Growth of Congruently Melting Gadolinium Scandium Gallium Garnet, J. Cryst. Growth 80 (1987) 26, https://doi.org/10.1016/0022-0248(87)90519-7.
[38] D. Mateika, E. Völkel, J. Haisma, Lattice-Constant-Adaptable Crystallographics. II. Czochralski Growth from Multicomponent Melts of Homogeneous Mixed-Garnet Crystals, J. Cryst. Growth 102 (1990) 994, https://doi.org/10.1016/0022-0248(90)90870-Q.